23. Pandori, M. W. *et al.* Producer-cell modification of human immunodeficiency virus type 1: Nef is a virion protein. *J. Virol.* **70,** 4283–4290 (1996).
24. Welker, R., Harris, M., Cardel, B. & Krausslich, H. G. Virion incorporation of human immunodeficiency virus type 1 Nef is mediated by a bipartite membrane-targeting signal: analysis of its role in enhancement of viral infectivity. *J. Virol.* **72,** 8833–8840 (1998).
25. Cohen, E. A., Subbramanian, R. A. & Gottlinger, H. G. Role of auxiliary proteins in retroviral morphogenesis. *Curr. Top. Microbiol. Immunol.* **214,** 219–235 (1996).
26. Madani, N. & Kabat, D. An endogenous inhibitor of human immunodeficiency virus in human lymphocytes is overcome by the viral Vif protein. *J. Virol.* **72,** 10251–10255 (1998).
27. Simon, J. H. & Malim, M. H. The human immunodeficiency virus type 1 Vif protein modulates the postpenetration stability of viral nucleoprotein complexes. *J. Virol.* **70,** 5297–5305 (1996).
28. Simon, J. H. *et al.* The regulation of primate immunodeficiency virus infectivity by Vif is cell species restricted: a role for Vif in determining virus host range and cross-species transmission. *EMBO J.* **17,** 1259–1267 (1998).
29. Kozak, M. Interpreting cDNA sequences: some insights from studies on translation. *Mamm. Genome* **7,** 563–574 (1996).
30. Folks, T. M. *et al.* Tumor necrosis factor α induces expression of human immunodeficiency virus in a chronically infected T-cell clone. *Proc. Natl Acad. Sci. USA* **86,** 2365–2368 (1989).

Supplementary Information accompanies the paper on *Nature*'s website (http://www.nature.com).

Acknowledgements

Vif monoclonal antibody (TG001; Transgene) and Nef monoclonal antibody (EH1; gift of J. Hoxie) were provided by the AIDS Research and Reference Reagent Program, Division of AIDS, NIAID, National Institutes of Health. We thank J. Kucinski and F. Calayag for technical assistance; M. Hayden, T. Liegler, R. Grant and the Gladstone Institute, San Francisco, for assistance with HIV-infected cells; V. Kewalramani, D. Littman, M. Goldsmith and W. Hansen for advice or, reagents; L. Caldwell and the Electron Microscopy Laboratory at the Fred Hutchinson Cancer Research Center in Seattle; and V. Lingappa, J. Lingappa, J. Dooher, J. Overbaugh, J. M. McCune, M. Linial and R. Hegde for discussions. This work was supported by grants to J.R.L. from the National Institutes of Health AIDS Division, Pediatric AIDS Foundation, and the University of California Universitywide AIDS Research Program.

Competing interests statement

The authors declare that they have no competing financial interests.

Correspondence and requests for materials should be addressed to J.R.L. (e-mail: jais@u.washington.edu). The sequence for WGHP68 has been deposited in GenBank under accession number AY059462.

IRE1 couples endoplasmic reticulum load to secretory capacity by processing the *XBP-1* mRNA

Marcella Calfon, Huiqing Zeng, Fumihiko Urano, Jeffery H. Till, Stevan R. Hubbard, Heather P. Harding, Scott G. Clark & David Ron

Skirball Institute of Biomolecular Medicine, New York University School of Medicine, New York, New York 10016, USA

The unfolded protein response (UPR), caused by stress, matches the folding capacity of endoplasmic reticulum (ER) to the load of client proteins in the organelle[1,2]. In yeast, processing of *HAC1* mRNA by activated Ire1 leads to synthesis of the transcription factor Hac1 and activation of the UPR[3]. The responses to activated IRE1 in metazoans are less well understood. Here we demonstrate that mutations in either *ire-1* or the transcription-factor-encoding *xbp-1* gene abolished the UPR in *Caenorhabditis elegans*. Mammalian *XBP-1* is essential for immunoglobulin secretion and development of plasma cells[4], and high levels of *XBP-1* messenger RNA are found in specialized secretory cells[5]. Activation of the UPR causes IRE1-dependent splicing of a small intron from the *XBP-1* mRNA both in *C. elegans* and mice. The protein encoded by the processed murine *XBP-1* mRNA accumulated during the UPR, whereas the protein encoded by unprocessed mRNA did not. Purified mouse IRE1 accurately cleaved *XBP-1* mRNA *in vitro*, indicating that *XBP-1* mRNA is a direct target of IRE1 endonucleolytic activity. Our findings suggest that physiological ER load regulates a developmental decision in higher eukaryotes.

IRE1 is a stress-activated endonuclease resident in the ER that is conserved in all known eukaryotes. In yeast, Ire1-mediated unconventional splicing of an intron from HAC1 mRNA controls expression of the encoded transcription factor[3] and is required for upregulation of most UPR target genes[6,7]. UPR gene expression in mammals relies largely on pancreatic ER kinase (PERK) and ATF6 (refs 8–11), which are absent from yeast. Furthermore, mammalian IRE1 proteins activate Jun amino-terminal kinase by recruiting the TRAF2 protein to the ER membrane independently of their endonucleolytic activity[12]. It is unclear, therefore, whether IRE1 proteins of higher eukaryotes also signal ER stress through processing of *HAC1*-like mRNA targets. To address this issue we used a genetic strategy to identify UPR regulatory genes in *C. elegans*, a simple organism whose genome is predicted to encode homologues of all three known proximal, stress-sensing components of the metazoan UPR: *IRE1*, *PERK* and *ATF6*.

Caenorhabditis elegans has two homologues of the ER chaperone

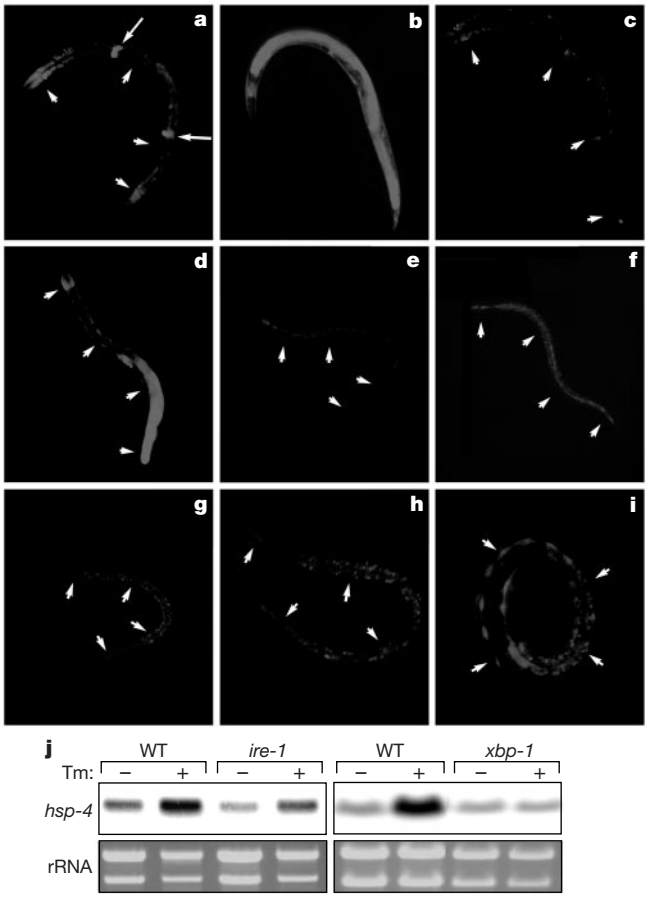

Figure 1 Identifying mutants in the *C. elegans* UPR. **a**, Fluorescent photomicrograph of an untreated adult *hsp-4::gfp(zcls4)V* transgenic animal. White arrowheads (in all panels) track the outline of the body; arrows indicate the spermatheca. **b**, An *hsp-4::gfp(zcls4)V* animal treated with tunicamycin. **c**, Tunicamycin-treated *ire-1(RNAi)II;hsp-4::gfp(zcls4)V* animal. **d**, Untreated *hsp-4::gfp(zcls4)V; upr-1(zc6)X* animal (note constitutive activation of the UPR in the posterior gut). **e**, Untreated *hsp-4::gfp(zcls4)V; upr-1(zc6)X* animal with a second mutation in *ire-1(zc14)II*. **f**, Tunicamycin-treated *ire-1(zc14)II; hsp-4::gfp(zcls4)V* animal. **g**, Untreated *hsp-4::gfp(zcls4)V; upr-1(zc6)X* animal with a second mutation in *xbp-1(zc12)III*. **h**, Tunicamycin-treated *xbp-1(zc12)III; hsp-4::gfp(zcls4)V* animal. **i**, Tunicamycin-treated *xbp-1(RNAi)III; hsp-4::gfp(zcls4)V* animal. **j**, Northern blot of *hsp-4* RNA from untreated and tunicamycin-treated (Tm) wild-type (WT), *ire-1(zc10)II* or *xbp-1(zc12)III* mutant animals. Integrity and loading of the RNA is revealed by ethidium bromide staining of the ribosomal bands. rRNA, ribosomal RNA.

BiP, *hsp-3* and *hsp-4*. An *hsp-4::gfp* transcriptional reporter had relatively low basal green fluorescent protein (GFP) expression (most prominent in the spermatheca, Fig. 1a), but expression was strongly induced in the gut and hypodermis after treatment with tunicamycin—a drug that induces ER stress (Fig. 1b). Inactivation of *ire-1* function by RNA interference (RNAi) blocked both basal and inducible *hsp-4::gfp* expression (Fig. 1c), suggesting that *ire-1* signalling is required for *hsp-4* induction in *C. elegans*, as it is in yeast. To identify the genes required for the UPR, we sought mutations that blocked induction of the *hsp-4::gfp* reporter. Because treatment with tunicamycin occasionally produced variable and incomplete *hsp-4::gfp* induction, we first isolated several mutations that constitutively activated *hsp-4::gfp* expression, presumably by causing ER stress. One semi-dominant mutation, *upr-1(zc6)X*, uniformly activated *hsp-4::gfp* in the posterior gut (Fig. 1d). We confirmed that *ire-1* RNAi suppressed *hsp-4::gfp* activation by *upr-1 (zc6)X* mutants (data not shown), and then we screened for mutations that blocked this activation.

We found four *ise-1* mutations that impaired *hsp-4::gfp* induction (Fig. 1e, f, j): *zc10* and *zc11* alter the 3′ splice acceptor site of intron 2, and *zc13* and *zc14* are missense mutations that affect conserved residues in the kinase domain (G702D and G739R, respectively). A fifth mutation, *zc12*, that strongly blocked *hsp-4::gfp* gene induction (Fig. 1g, h, j) mapped to the interval between cosmid F34D10 and *dpy-17* on chromosome III. A plausible candidate for a downstream target of *ire-1*—a predicted basic leucine zipper (bZIP) transcription factor gene, *R74.3*—was located in this interval. Sequence analysis of *zc12* mutants revealed a single nonsense mutation at residue 11 in the predicted R74.3 protein, and RNAi of R74.3 inhibited *hsp-4::gfp* induction (Fig. 1i). Together, these results indicate that R74.3 has an essential role in *C. elegans* UPR.

The predicted R74.3 protein of *C. elegans* is most similar to mouse XBP-1 (X-box binding protein-1), which binds the BiP ER

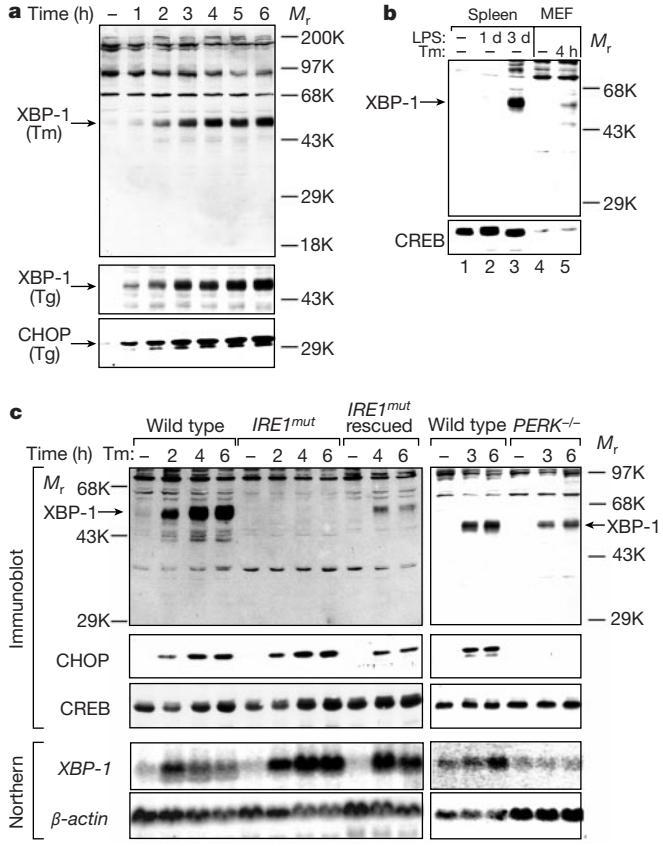

Figure 2 Mammalian XBP-1 expression during ER stress is dependent on IRE1. **a**, XBP-1 immunoblot from murine fibroblasts treated with tunicamycin (Tm, upper panel) or thapsigargin (Tg, middle panel). CHOP immunoblot of the thapsigargin-treated lysates provides a positive control for the induction of the UPR (lower panel). **b**, XBP-1 immunoblot of lysates of differentiating mouse spleen cells cultured in medium with or without bacterial lipopolysaccharide (LPS) for the indicated number of days, and lysates of untreated and tunicamycin-treated fibroblasts. CREB (lower panel) serves as a loading and recovery control. MEF, mouse embryonic fibroblast. **c**, XBP-1, CHOP and CREB immunoblots and *XBP-1* and *β-actin* northern blots from untreated and tunicamycin-treated cells with the indicated genotypes.

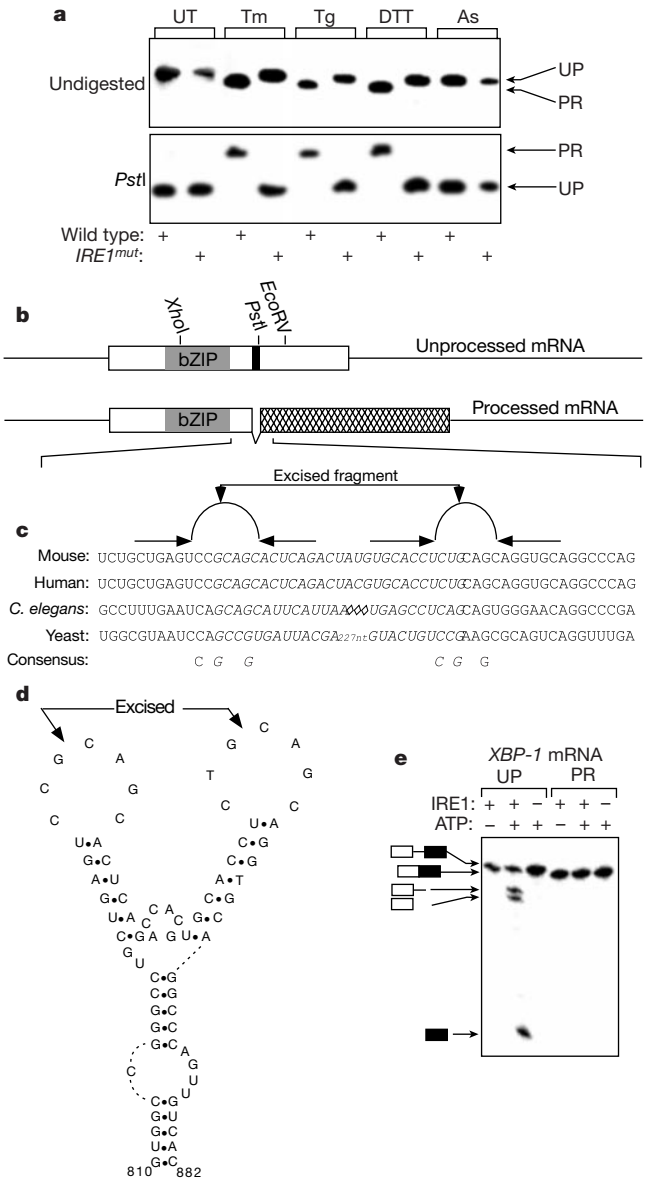

Figure 3 IRE1-mediated processing of *XBP-1* mRNA. **a**, Autoradiogram of a Southern blot of undigested or *Pst*1-digested *XBP-1* cDNA from wild-type or *IRE1* mutant cells that were untreated (UT) or treated with tunicamycin (Tm), thapsigargin (Tg), dithiothreitol (DTT) or sodium arsenite (As). The unprocessed (UP) and processed (PR) cDNA fragments are indicated by the arrows to the left of the autoradiograms. **b**, Map of the unprocessed and processed murine *XBP-1* mRNAs. The coding regions are boxed, the bZIP domain is shaded grey and the intron excised by IRE1 is coloured black. The ORF in the processed mRNA is hatched. **c**, Alignment of the RNA sequence surrounding the intron in mouse, human and *C. elegans XBP-1*, and yeast *HAC1*. The predicted stem-loop structures cleaved by IRE1 are represented by opposing arrows (stems) flanking the semicircle (loop). Conserved residues in the loops are indicated by the consensus sequence. **d**, Predicted secondary structure of the mouse *XBP-1* mRNA in the region surrounding the IRE1 cleavage sites (arrows). **e**, Autoradiogram of radiolabelled fragments produced by site-specific cleavage of the unprocessed (UP) or processed (PR) *XBP-1* mRNA by purified IRE1 *in vitro*.

stress-response element[13]. Therefore, we investigated further the regulation of XBP-1 in the mammalian UPR. ER stress induced a protein with a relative molecular mass of 54,000 (M_r 54K) that was strongly reactive with antiserum to XBP-1 (Fig. 2a). The 54K XBP-1 protein was also induced during *in vitro* differentiation of B cells to plasma cells by exposure to bacterial lipopolysaccharide (Fig. 2b). Thus, ER stress- and differentiation-induced remodelling of the secretory apparatus are both associated with XBP-1 expression.

Mice have two *IRE1* genes: *IRE1*α is essential for viability and is broadly expressed[12,14], and *IRE1*β is expressed only in the gastrointestinal mucosa[15,16]. Induction of the 54K XBP-1 protein by ER stress was not observed in fibroblasts that lacked IRE1 gene function ($IRE1\alpha^{-/-}$ or $IRE1\alpha\beta^{-/-}$) but could be rescued by introduction of an *IRE1* transgene (Fig. 2c). ER stress has been shown to increase levels of *XBP-1* mRNA[10]. However, *IRE1* mutant cells that do not express the 54K XBP-1 protein had higher levels of *XBP-1* mRNA than wild-type cells (Fig. 2c, lower panels). Furthermore, $PERK^{-/-}$ cells that failed to induce *XBP-1* mRNA accumulate 54K XBP-1 protein when stressed (albeit to lower levels than wild-type cells, Fig. 2c). IRE1 activity is thus required for expression of XBP-1, whereas ER-stress-mediated increase in *XBP-1* mRNA is less important in this process.

To investigate possible IRE1-mediated processing of *XBP-1* mRNA, we performed polymerase chain reaction with reverse transcription (RT-PCR) of *XBP-1* mRNA from unstressed and stressed wild-type and *IRE1*-mutant mouse cells. We found a consistent *IRE1* and ER stress-dependent decrease in the size of the *Xho*I–*Eco*RV fragment of the *XBP-1* complementary DNA (Fig. 3a). Sequencing revealed excision of a 26-nucleotide intron from the *XBP-1* cDNA derived from stressed wild-type cells (Fig. 3b, c). A similarly located 23-nucleotide intron was removed by ER stress from the *C. elegans xbp-1* mRNA (Fig. 3c, and data not shown). The boundaries of these introns were encompassed in a predicted RNA structure that included two loops of seven residues held in place by short stems (Fig. 3c, d). The sequence of the loops corresponded perfectly to the empirically defined consensus sequence for cleavage of yeast *HAC1* mRNA by Ire1 (refs 17, 18). The RNA sequences 5′ and 3′ to these two putative processing sites are predicted to form extensive base-pair interactions that could hold together the cleaved ends of the mRNA (Fig. 3d), as has been predicted for the *HAC1* mRNA[17].

To study the role of IRE1 in the processing of *XBP-1* mRNA, we reconstructed the cleavage event *in vitro*. The cytoplasmic effector domain of murine IRE1β was purified from insect cells and reacted *in vitro* with a transcribed, unprocessed *XBP-1* mRNA that had been radiolabelled ($XBP\text{-}1^{up}$), or with *XBP-1* mRNA transcribed from a processed cDNA template ($XBP\text{-}1^{pr}$). IRE1β efficiently cleaved $XBP\text{-}1^{up}$ RNA in an ATP-dependent manner but did not cleave $XBP\text{-}1^{pr}$ (Fig. 3e). The location of the *in vitro* cleavage sites was mapped by primer extension and found to coincide with the sites used *in vivo* (Supplementary Information Fig. 1).

Re-ligation of *XBP-1* mRNA after removal of the 26-nucleotide intron results in a shift of the reading frame and continuation of the protein-coding region into the former 3′ untranslated region (Fig. 3b). The protein predicted by the extended open reading frame (ORF) of the processed *XBP-1* mRNA ($XBP\text{-}1^{pr}$) is similar in size to the 54K XBP-1 protein detected in stressed cells. To explore further the relationship between processing of the *XBP-1* mRNA and expression of the 54K protein, we modified both processed and unprocessed *XBP-1* cDNAs to encode N-terminal Flag-tagged proteins, and studied their expression in transfected cells. Human embryonic kidney (HEK) 293T cells transfected with the processed *XBP-1* cDNA constitutively expressed high levels of the 54K XBP-1

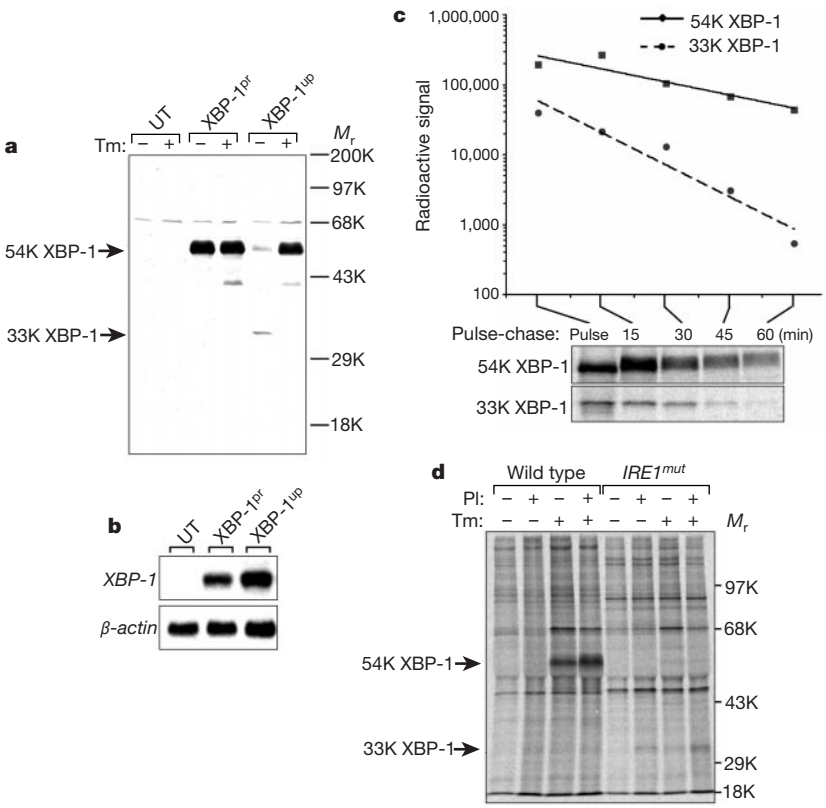

Figure 4 Processing of *XBP-1* mRNA controls expression of the encoded protein. **a**, Immunoblot of N-terminal Flag-tagged XBP-1 from untreated or tunicamycin-treated (Tm) untransfected (UT) cells and cells transfected with expression plasmids containing the processed ($XBP\text{-}1^{pr}$) or unprocessed ($XBP\text{-}1^{up}$) *XBP-1* cDNA. **b**, Northern blot of mouse *XBP-1* mRNA from the transfected cells. **c**, Autoradiogram of a pulse-chase experiment of metabolically labelled Flag-tagged XBP-1 proteins from transfected cells, and the corresponding logarithmic plot of the radioactive protein signal intensity as a function of time. **d**, Autoradiogram of metabolically labelled endogenous XBP-1 proteins from untreated, tunicamycin-treated (Tm) and proteasome-inhibited (PI) wild-type and *IRE1* mutant mouse fibroblasts.

protein (Fig. 4a). By contrast, cells transfected with *XBP-1*^{up} expressed only low levels of a Flag-tagged protein of 33K, consistent in size with the ORF specified by the unprocessed mRNA. On treatment with tunicamycin, cells transfected with *XBP-1*^{up} expressed high levels of the Flag-tagged 54K protein (Fig. 4a). These observations indicate that the protein encoded by the unprocessed mRNA was poorly expressed and that processing of the exogenous mRNA by endogenous IRE1 led to the expression of the 54K XBP-1 protein.

We performed pulse-chase experiments to explore the basis of the differences in expression of proteins encoded by the transfected *XBP-1*^{up} and *XBP-1*^{pr} mRNAs, as northern blot analysis showed similar levels of the two mRNAs (Fig. 4b). Using a short (10 min) labelling pulse, we found that the level of 54K XBP-1 accumulation was 4-fold higher than that for 33K XBP-1; the half-life of the 54K XBP-1 protein was twice that of 33K XBP-1 (22 min and 11 min, respectively). On the basis of these measurements, the synthesis rate of the 54K XBP-1 protein is 3.46-fold higher than that of 33K XBP-1. Furthermore, endogenous 54K XBP-1 accumulated to high levels in pulse-labelled wild-type cells that were treated with tunicamycin, whereas labelled 33K XBP-1 protein was barely detectable (Fig. 4d). The 33K XBP-1 signal was more obvious in IRE1 mutant cells, presumably because they accumulate *XBP-1*^{up} mRNA (Fig 2c). Levels of the 33K XBP-1 protein increased further in cells treated with a proteasome inhibitor (Fig. 4d, see also Supplementary Information Fig. 2), consistent with the short half-life of the protein. The half-life of endogenous 54K XBP-1 protein was approximately 21 min, similar to that of the over-expressed protein; however, the weak incorporation of label precluded accurate measurement of the half-life of endogenous 33K XBP-1 protein (Supplementary Information Fig. 2).

As in the regulation of *HAC1* in yeast, mammalian IRE1 acts as a site-specific endonuclease to cleave the mRNA of a bZIP transcription factor. Cleavage and removal of a small intron is followed by re-ligation of the 5′ and 3′ fragments to produce a processed mRNA that is translated more efficiently and encodes a more stable protein. These findings provide new insight into the organization and evolution of the metazoan UPR. In yeast, virtually all genes activated in the UPR are *IRE1*- and *HAC1*-dependent[6,7]. Nematodes lacking *ire-1* or *xbp-1* function are also unable to induce *hsp-4* (*BiP*) and other target genes of the UPR (Fig. 1j and data not shown). By contrast, *IRE1* mutant mammalian cells have no obvious defect in inducing UPR markers such as *CHOP* (C/EBP homologous protein) or *XBP-1* itself (Fig. 2c). It seems that mammalian evolution was associated with specialization of IRE1 and XBP-1 function, diverting these proteins from control of many UPR target genes towards certain specific cellular functions. The phenotype of the *XBP-1*$^{-/-}$ mouse may provide a clue to the nature of that specialization. *RAG1*$^{-/-}$ (recombinase-activating gene 1) mice whose lymphoid system has been reconstituted with *XBP-1*$^{-/-}$ cells have a profound defect in immunoglobulin secretion, which reflects impaired differentiation of B cells to plasma cells[4]. The distinction between a plasma cell and B cell is based on acquisition of the ability to secrete large amounts of immunoglobulin and its morphological corollary, an elaborate ER. Our finding that IRE1 controls XBP-1 expression suggests, therefore, that increased load of client proteins in the ER activates XBP-1 and triggers development of an elaborate secretory apparatus—the hallmark of a plasma cell. □

Methods

Analysis of the UPR in *C. elegans*

A 1.1-kilobase (kb) fragment of *C. elegans* genomic DNA immediately 5′ of the predicted initiation ATG codon of *hsp-4* was amplified by PCR and ligated in-frame with GFP in the plasmid pPD95.75 (gift of A. Fire). We generated the *hsp-4::gfp(zcIs4)V* strain by co-injecting the *hsp-4::gfp* clone with the *lin-15* rescuing plasmid, pSK1 (ref. 19), into *lin-15(n765ts)* animals and then integrating the extrachromosomal array with ultraviolet/trimethylpsoralen treatment. We screened the F_2 progeny of ethylmethane sulphonate (EMS)-treated *hsp-4::gfp(zcIs4)V* animals for mutants with high levels of GFP expression to identify mutations that constitutively induce the UPR. Several mutations were recovered, including *upr-1(zc6)X,* which induced a high level of GFP expression in the posterior gut. To isolate mutations that blocked induction of *hsp-4::gfp*, we screened the F_2 progeny of EMS-treated *hsp-4::gfp(zcIs4)V; upr-1(zc6)X* animals for mutants with a reduced GFP signal. We mapped the mutations to visible markers and single nucleotide polymorphic markers.

RNAi was performed by injecting double-stranded RNA—made *in vitro* through using as a template the 720-bp *Sal*I–*Eco*RI fragment of the *ire-1* cDNA (clone yk8e9) or the 515-bp *Sal*I–*Nco*I fragment of the *xbp-1* cDNA (clone yk146d1)—into young adult hermaphrodites, and then observing the phenotype of the F_1 progeny as described previously[20]. We transferred animals to plates containing 5 μg ml^{-1} tunicamycin (Calbiochem), and visualized the GFP expression using an epifluorescent stereomicroscope (Zeiss M2 Bio). RNA for northern blot analysis was isolated by acid-guanidinium thiocyanate-phenol-chloroform extraction. We used a radiolabelled 100-bp *Hin*dIII–*Xho*I fragment from *hsp-4* cDNA clone yk34e10 as a probe.

Cell culture, transfection, immunoblot and immunoprecipitation

Mouse embryonic fibroblasts and embryonic stem cells lacking *IRE1* activity (*IRE1α*$^{-/-}$ or *IRE1α*; *IRE1β*$^{-/-}$), and *PERK*$^{-/-}$ fibroblasts were cultured as described previously[9,12]. Cells were treated with tunicamycin (2.5 μg ml^{-1}; Calbiochem), thapsigargin (100 nM; Sigma), dithiothreitol (2 mM; Sigma) or the proteasome inhibitor MG132 (25 μM; Calbiochem), as indicated. To activate B-cell differentiation *in vitro* cells were teased from crushed adult mouse spleen and cultured in the presence of 25 μg ml^{-1} *Escherichia coli* lipopolysaccharide.

We purchased a full-length murine *XBP-1* cDNA (expressed sequence tag BF454459, Research Genetics). The processed version of the cDNA was created by replacing the *Xho*I–*Eco*RV fragment of the unprocessed cDNA with the equivalent fragment from the processed cDNA obtained by RT-PCR of mRNA from stressed cells. Flag-tagged versions of the two cDNAs were constructed by inserting the Flag epitope tag sequence immediately 3′ of the ATG start codon, and the cDNAs were expressed from a plasmid containing the human cytomegalovirus virus (CMV) promoter (pFlag-CMV2).

XBP-1 proteins in whole-cell extracts were detected by an immunoblot of 9% SDS–polyacrylamide gel electrophoresis (PAGE) using a rabbit polyclonal serum directed to residues 97–267, common to both 54K and 33K XBP-1 proteins (sc-8015; Santa Cruz Biotechnology). XBP-1 proteins in transfected cells were detected by a monoclonal antibody to the Flag epitope tag (Kodak-IBI). The transcription factors CREB and CHOP were detected as described previously[9].

Newly synthesized proteins were labelled *in vivo* with ^{35}S-methionine and ^{35}S-cysteine (500 μCi ml^{-1}, Translabel, ICN Biochemicals). After removal of the labelling medium cells were washed and incubated in complete medium for cold chase. Labelled XBP-1 proteins from whole-cell extracts prepared in radio-immunoprecipitation buffer[9] were immunoprecipitated using the anti-Flag or anti-XBP-1 antibodies described above and revealed by autoradiography after 9% SDS–PAGE. Incorporation of the radiolabel was quantified by phosphoimager analysis. In calculating the relative synthesis rates of 54K XBP-1 and 33K XBP-1, the relative incorporation of label was corrected for differences in the content of methionine (7:6) and cysteine (4:3) predicted for the two proteins.

Analysis of XBP-1 mRNA cleavage by IRE1

RNA from untreated and tunicamycin-treated wild-type and *IRE1α*$^{-/-}$ mouse embryonic stem cells was reverse transcribed using an *XBP-1*-specific antisense primer, mXBP1.4AS: 5′-GCACCTTCTAGAAGCTACACTAGCA-3′. Nested PCR using the sense primer mXBP1.3S (5′-AAACAGAGTAGCAGCGCAGACTGC-3′) and the antisense primer mXBP1.2AS: (5′-GGATCTCTAAAACTAGAGGCTTGGTG-3′) amplified a 600-bp cDNA product encompassing the IRE1 cleavage sites. This fragment was further digested by *Pst*I to reveal a restriction site that is lost after IRE1-mediated cleavage and splicing of the mRNA. The cDNA fragments were resolved on a 2% agarose gel and revealed by Southern blot hybridized to the ^{32}P-labelled *Xho*I–*Pst*I fragment of the unprocessed *XBP-1* cDNA. The processed cDNAs from mouse and *C. elegans* were sequenced and the sequence deposited in GenBank under accession numbers AF443192 and AF443191, respectively.

The *Xho*I–*Eco*RV fragment of the XBP-1 cDNA from unstressed (*XBP-1*^{up}) and stressed (*XBP-1*^{pr}) mouse embryonic stem cells was ligated into pBluescript plasmid (Stratagene) and sense strand ^{32}P-labelled RNA was transcribed *in vitro* using a kit from Promega. The labelled RNA was incubated in the presence or absence of 1 mM ATP with the recombinant cytoplasmic domain of IRE1β purified from SF9 cells as described[21]. The radiolabelled RNA fragments were resolved on 8 M urea 6% PAGE gel and revealed by autoradiography.

Received 28 August; accepted 23 November 2001.

1. Mori, K. Tripartite management of unfolded proteins in the endoplasmic reticulum. *Cell* **101,** 451–454 (2000).
2. Kaufman, R. J. Stress signaling from the lumen of the endoplasmic reticulum: coordination of gene transcriptional and translational controls. *Genes Dev.* **13,** 1211–1233 (1999).
3. Shamu, C. E. Splicing: HACking into the unfolded-protein response. *Curr. Biol.* **8,** R121–R123 (1998).
4. Reimold, A. M. *et al.* Plasma cell differentiation requires the transcription factor XBP-1. *Nature* **412,** 300–307 (2001).
5. Clauss, I. M. *et al. In situ* hybridization studies suggest a role for the basic region-leucine zipper protein hXBP-1 in exocrine gland and skeletal development during mouse embryogenesis. *Dev. Dyn.* **197,** 146–156 (1993).
6. Travers, K. J. *et al.* Functional and genomic analyses reveal an essential coordination between the unfolded protein response and ER-associated degradation. *Cell* **101,** 249–258 (2000).

7. Casagrande, R. *et al.* Degradation of proteins from the ER of *S. cerevisiae* requires an intact unfolded protein response pathway. *Mol. Cell* **5,** 729–735 (2000).
8. Scheuner, D. *et al.* Translational control is required for the unfolded protein response and *in vivo* glucose homeostasis. *Mol. Cell* **7,** 1165–1176 (2001).
9. Harding, H. *et al.* Regulated translation initiation controls stress-induced gene expression in mammalian cells. *Mol. Cell* **6,** 1099–1108 (2000).
10. Yoshida, H. *et al.* ATF6 activated by proteolysis binds in the presence of NF-Y (CBF) directly to the *cis*-acting element responsible for the mammalian unfolded protein response. *Mol. Cell Biol.* **20,** 6755–6767 (2000).
11. Ye, J. *et al.* ER stress induces cleavage of membrane-bound ATF6 by the same proteases that process SREBPs. *Mol. Cell* **6,** 1355–1364 (2000).
12. Urano, F. *et al.* Coupling of stress in the endoplasmic reticulum to activation of JNK protein kinases by transmembrane protein kinase IRE1. *Science* **287,** 664–666 (2000).
13. Yoshida, H., Haze, K., Yanagi, H., Yura, T. & Mori, K. Identification of the *cis*-acting endoplasmic reticulum stress response element responsible for transcriptional induction of mammalian glucose-regulated proteins. Involvement of basic leucine zipper transcription factors. *J. Biol. Chem.* **273,** 33741–33749 (1998).
14. Tirasophon, W., Welihinda, A. A. & Kaufman, R. J. A stress response pathway from the endoplasmic reticulum to the nucleus requires a novel bifunctional protein kinase/endoribonuclease (Ire1p) in mammalian cells. *Genes Dev.* **12,** 1812–1824 (1998).
15. Bertolotti, A. *et al.* Increased sensitivity to dextran sodium sulfate colitis in IRE1b deficient mice. *J. Clin. Invest.* **107,** 585–593 (2001).
16. Wang, X. Z. *et al.* Cloning of mammalian Ire1 reveals diversity in the ER stress responses. *EMBO J.* **17,** 5708–5717 (1998).
17. Gonzalez, T. N., Sidrauski, C., Dorfler, S. & Walter, P. Mechanism of non-spliceosomal mRNA splicing in the unfolded protein response pathway. *EMBO J.* **18,** 3119–3132 (1999).
18. Kawahara, T., Yanagi, H., Yura, T. & Mori, K. Unconventional splicing of HAC1/ERN4 mRNA required for the unfolded protein response. Sequence-specific and non-sequential cleavage of the splice sites. *J. Biol. Chem.* **273,** 1802–1807 (1998).
19. Clark, S. G., Lu, X. & Horvitz, H. R. The *Caenorhabditis elegans* locus lin-15, a negative regulator of a tyrosine kinase signaling pathway, encodes two different proteins. *Genetics* **137,** 987–997 (1994).
20. Fire, A. *et al.* Potent and specific genetic interference by double-stranded RNA in *Caenorhabditis elegans*. *Nature* **391,** 806–811 (1998).
21. Niwa, M., Sidrauski, C., Kaufman, R. J. & Walter, P. A role for presenilin-1 in nuclear accumulation of Ire1 fragments and induction of the mammalian unfolded protein response. *Cell* **99,** 691–702 (1999).

Supplementary Information accompanies the paper on *Nature*'s website (http://www.nature.com).

Acknowledgements

We thank C. Chiu for help in initiating the nematode work; A. Bertolotti, D. Levy and E. Y. Skolnik for useful discussions; Y. Kohara for *C. elegans* EST clones; and A. Ron and R. Onn for calculating the synthesis rate of XBP1 proteins. This work was supported by grants from the National Institutes of Health. D.R. is a Scholar of the Ellison Medical Foundation.

Competing interests statement

The authors declare that they have no competing financial interests.

Correspondence and requests for materials should be addressed to D.R. (e-mail: ron@saturn.med.nyu.edu).

Superoxide activates mitochondrial uncoupling proteins

Karim S. Echtay*, Damien Roussel*, Julie St-Pierre*, Mika B. Jekabsons*, Susana Cadenas*, Jeff A. Stuart*, James A. Harper*, Stephen J. Roebuck*, Alastair Morrison†, Susan Pickering†, John C. Clapham‡ & Martin D. Brand*

** Medical Research Council Dunn Human Nutrition Unit, Hills Road, Cambridge CB2 2XY, UK*
Departments of †Comparative Genomics, and ‡ Vascular Biology, GlaxoSmithKline, Harlow, Essex CM19 5AW, UK

Uncoupling protein 1 (UCP1) diverts energy from ATP synthesis to thermogenesis in the mitochondria of brown adipose tissue by catalysing a regulated leak of protons across the inner membrane[1,2]. The functions of its homologues, UCP2 and UCP3, in other tissues are debated[3,4]. UCP2 and UCP3 are present at much lower abundance than UCP1, and the uncoupling with which they are associated is not significantly thermogenic[5,6]. Mild uncoupling would, however, decrease the mitochondrial production of reactive oxygen species, which are important mediators of oxidative damage[7,8]. Here we show that superoxide increases mitochondrial proton conductance through effects on UCP1, UCP2 and UCP3. Superoxide-induced uncoupling requires fatty acids and is inhibited by purine nucleotides. It correlates with the tissue expression of UCPs, appears in mitochondria from yeast expressing UCP1, and is absent in skeletal muscle mitochondria from UCP3 knockout mice. Our findings indicate that the interaction of superoxide with UCPs may be a mechanism for decreasing the concentrations of reactive oxygen species inside mitochondria.

As coenzyme Q (CoQ) has been identified as a regulatory cofactor for proton transport by UCP1 (ref. 9), UCP2 and UCP3 (ref. 10) in liposomes, we tested the effect of CoQ in isolated mitochondria. CoQ increased proton conductance in rat kidney (but not liver) mitochondria that were oxidizing succinate. This increase required fatty acids and was prevented by GDP. CoQ activated proton conductance only when it was likely to be reduced to $CoQH_2$. Activation was abolished by superoxide dismutase, indicating that CoQ might mediate uncoupling through the production of superoxide[11]. To explore this possibility, we replaced CoQ by xanthine plus xanthine oxidase—an exogenous system that generates superoxide. Proton conductance increased, indicating that CoQ acted in mitochondria through the production of superoxide.

Incubating rat skeletal muscle mitochondria with xanthine plus xanthine oxidase to generate superoxide increased proton conductance (Fig. 1a). This is seen as an increased rate of proton leak at each membrane potential, resulting in a curve that is deflected upwards. This increase was fully inhibited either by superoxide dismutase, indicating that it was dependent on superoxide, or by 500 μM GDP (Fig. 1a). GDP had no effect on control mitochondria (data not shown), confirming previous results[12].

The superoxide effect was abolished by bovine serum albumin (BSA), which binds fatty acids (Fig. 1b), but restored by adding palmitic acid in the presence of BSA (Fig. 1c), indicating that activation by superoxide requires fatty acids. Proton conductance that is activated by fatty acids and sensitive to GDP is characteristic of uncoupling by UCP1 in brown adipose tissue (BAT) mitochondria[1,2], suggesting that the uncoupling caused by superoxide in skeletal muscle mitochondria (which lack UCP1 and -2 (ref. 13) but contain UCP3) was mediated by UCP3.

We also investigated skeletal muscle mitochondria from starved rats. Starvation for 24 h doubles the concentration of UCP3 protein without affecting the basal level of proton conductance[12]. Superoxide stimulated proton conductance twice as strongly in mitochondria from starved rats (Fig. 1d) as in mitochondria from fed rats (Fig. 1a). The same was true in the presence of BSA plus palmitate (data not shown). This correlates with a near doubling of UCP3 protein in starved rats, which was confirmed by western blot (data not shown), and implicates UCP3 in the superoxide effect.

Confirmation of the role of UCP3 was obtained using skeletal muscle mitochondria isolated from UCP3 knockout mice, which had the same basal proton conductance as the controls. Muscle mitochondria from wild-type mice showed the same GDP-sensitive stimulation of proton conductance as those from rats (Fig. 1e) and the same dependence on fatty acids (data not shown). However, superoxide had no effect on mitochondria from the skeletal muscle of UCP3 knockout mice (Fig. 1f), showing that superoxide uncoupled wild-type mitochondria by interacting with UCP3. We verified that the lack of effect of xanthine plus xanthine oxidase in UCP3 knockouts was not caused by lack of superoxide by a direct assay of superoxide production using superoxide dismutase and a homovanillic acid/horseradish peroxidase fluorescence assay[14] (data not shown). Thus, the fatty-acid-dependent, GDP-sensitive increase in proton conductance caused by xanthine plus xanthine oxidase

Supplemental material

Supplemental Methods:

Mapping the in vitro cleavage of mouse XBP-1 by IRE1:

The *Xho*I-*Eco*RV fragment of the XBP-1 cDNA from unstressed (*XBP-1*^{up}) and stressed (*XBP-1*^{pr}) mouse ES cells was ligated into pBluescript plasmid (Stratagene) which was then linearized with *Eco*R1 and sense strand ^{32}P-labeled RNA was transcribed in vitro using a kit from Promega. The labeled RNA was incubated in the presence or absence of 1mM ATP with the recombinant cytoplasmic domain of IRE1β purified from SF9 cells as described[21]. The radiolabeled RNA fragments were resolved on 8M urea 6% PAGE gel and revealed by autoradiography. To generate a sequencing ladder with nested fragments having the same ends as the labeled RNA fragments, we designed a primer that annealed to the pBluescript plasmid containing the aforementioned *Xho*I-*Eco*RV fragment of the XBP-1 cDNA at the predicted 5' overhang generated by *Eco*RI digestion. The ^{32}P-radiolabeled primer was used for both dideoxy-nucleotide sequencing of the plasmid and for primer extension of the in vitro digested XBP-1 mRNA.

Measuring the half-life of endogenous XBP-1pr:

Cells were left untreated or pretreated for 3 hours with tunicamycin (2.5μg/ml), followed by a short 10 minute labeling pulse and a chase of 30 and 60 minutes. Endogenous XBP-1 protein was immunoprecipitated using the rabbit anti-XBP-1 serum described above.

Supplemental Legends:

Supplemental figure 1:

Mapping the in vitro cleavage of mouse XBP-1 by IRE1. Autoradiogram of a sequencing gel on which the uncleaved and cleaved mRNA (prepared as for figure 3e) were resolved (lanes 5 and 6) alongside a cDNA sequencing ladder commencing at the 3' end of the labeled mRNA (lanes 1-4). Primer extension of the uncleaved mRNA (lane 7) or cleaved mRNA (lanes 8 & 9) with the same radiolabeled primer used to generate the sequencing ladder shown in lanes 1-4.

Supplemental figure 2:

Measuring the half-life of endogenous XBP-1^{pr} and detecting endogenous XBP-1^{up} by immunoblot: **a.** Autoradiogram of a pulse-chase experiment of metabolically-labeled endogenous XBP-1 proteins from untreated (UT) and tunicamycin-treated (Tm) wildtype cells. **b.** Immunoblot of endogenous XBP-1 proteins in wildtype and ***IRE1*** mutant mouse fibroblasts treated with the proteasomal inhibitor, MG132 or tunicamycin (Tm).

Calfon_Supplemental fig1

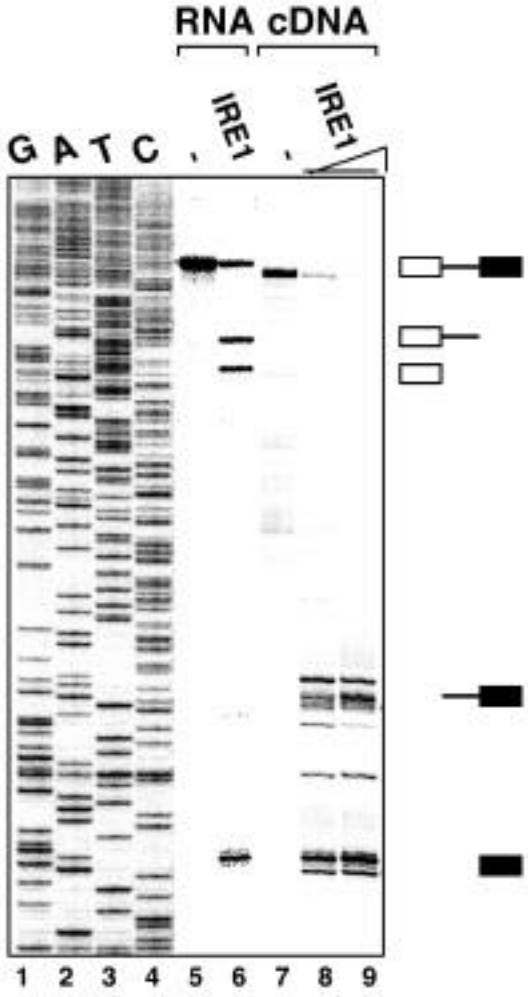

calfon_supplemental Fig 2